Supplemental Information

for

High-Performance Triboelectric Nanogenerators Incorporating Chlorinated Zeolitic Imidazolate Frameworks with Topologically Tunable Dielectric and Surface Adhesion Properties

Jiahao Ye [a] and Jin-Chong Tan [a*]

[a]Multifunctional Materials & Composites (MMC) Laboratory,
Department of Engineering Science, University of Oxford, Parks Road,
Oxford OX1 3PJ, U.K.

[*]Corresponding Author and Lead Contact, Email: jin-chong.tan@eng.ox.ac.uk

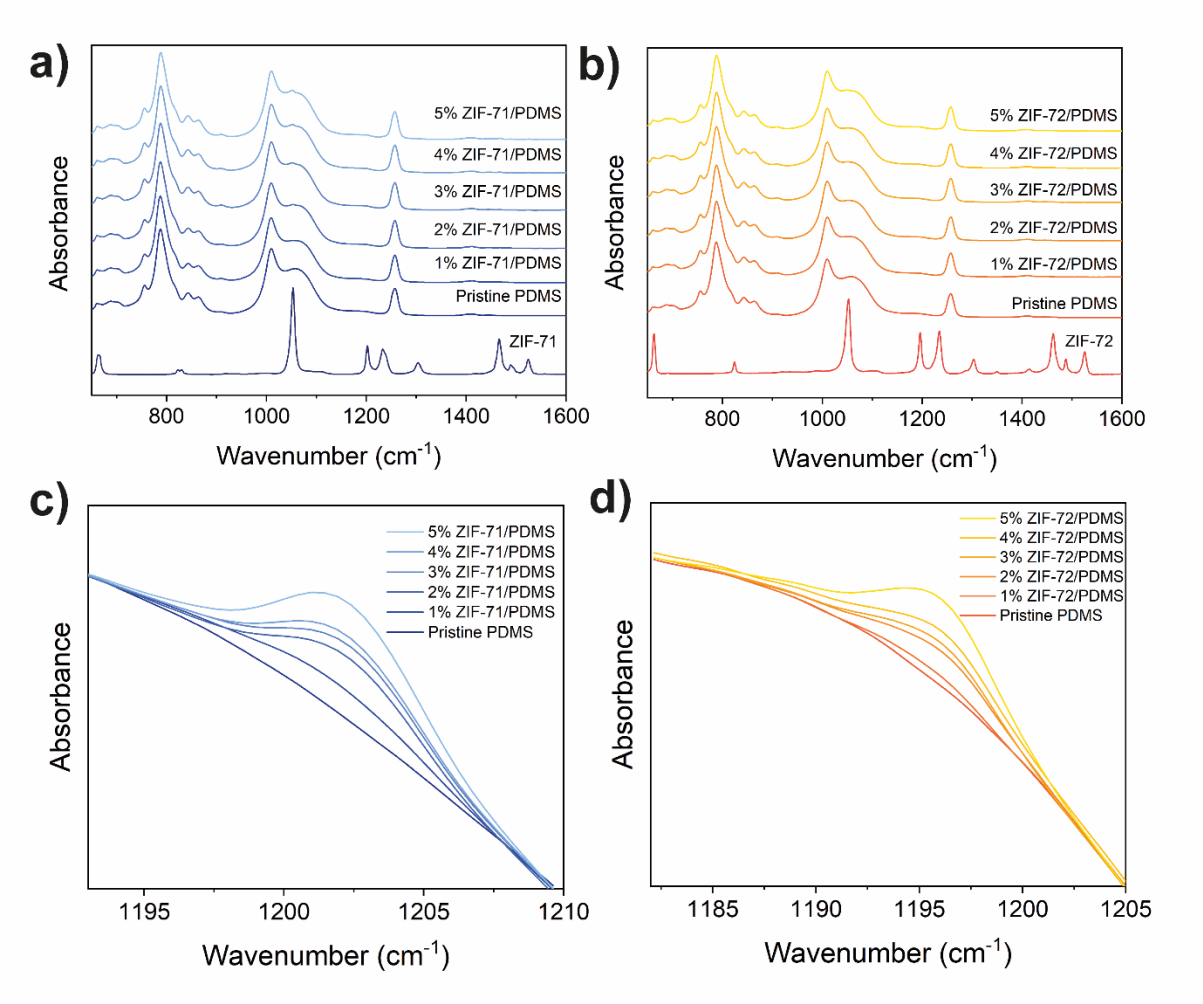

Fig. S1. a) FTIR spectra of ZIF-71 embedded PDMS films under different mass loadings (wt.%), compared with ZIF-71 nanoparticles. b) FTIR spectra of ZIF-72 embedded PDMS films under different mass loadings, compared with ZIF-72 nanoparticles. c) Superimposed FTIR spectra of ZIF-71/PDMS composites between 1192 cm^{-1} and 1210 cm^{-1}. d) FTIR spectra of ZIF-72/PDMS composites from 1182 cm^{-1} to 1205 cm^{-1}.

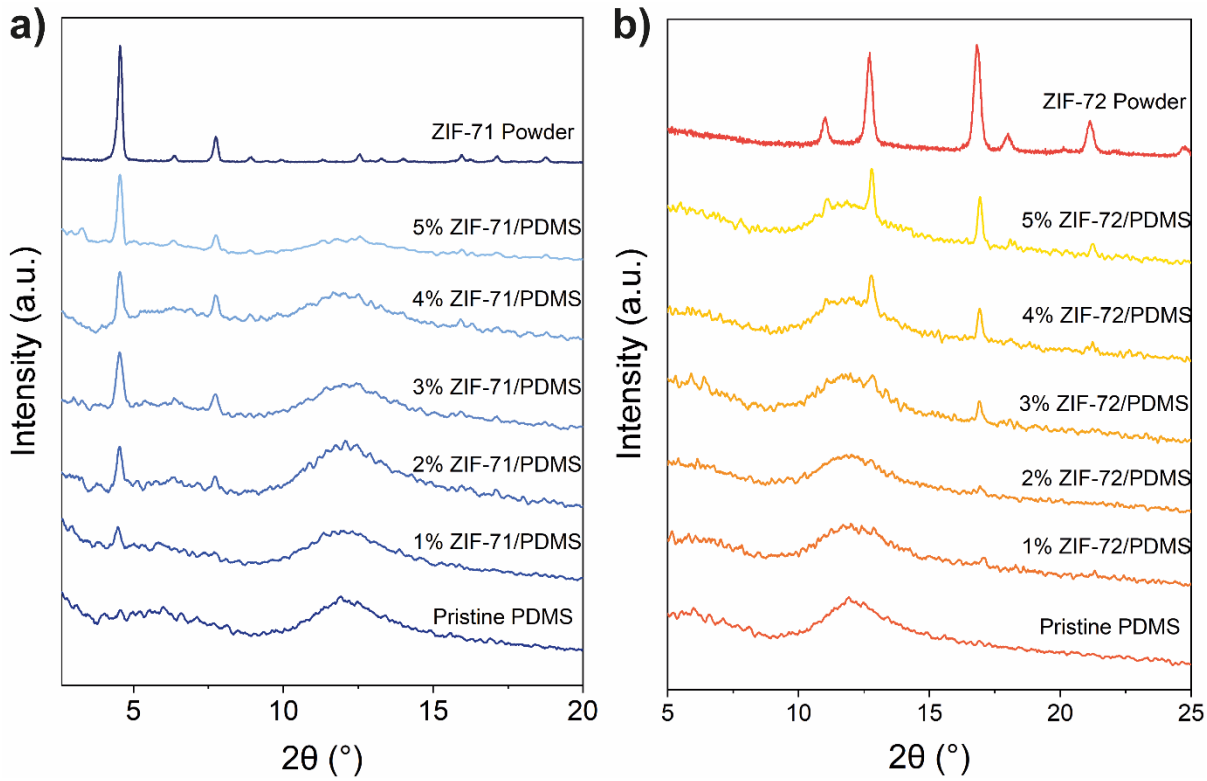

Fig. S2. a) XRD patterns of ZIF-71 embedded PDMS films under different mass loadings (wt.%), compared with ZIF-71 nanoparticles. b) XRD patterns of ZIF-72 embedded PDMS films under different mass loadings, compared with ZIF-72 nanoparticles.

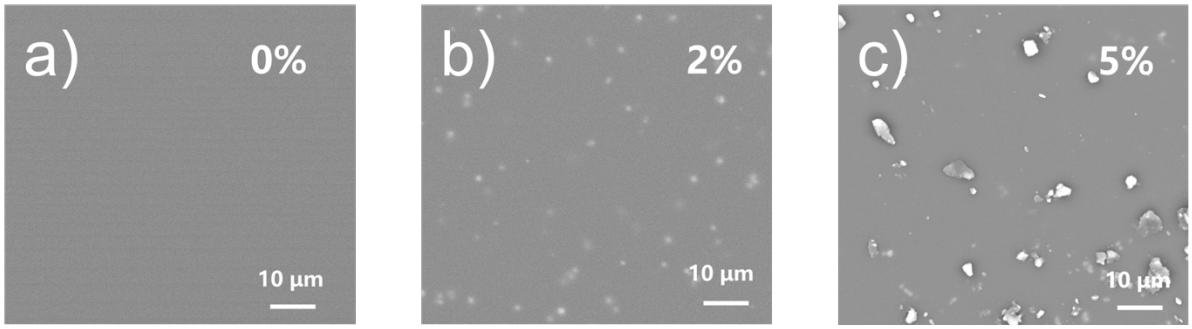

Fig. S3. SEM micrographs of the top surfaces of ZIF-71/PDMS nanocomposite films, containing a) 0 wt%, b) 2 wt%, and c) 5 wt% of ZIF-71filler loading.

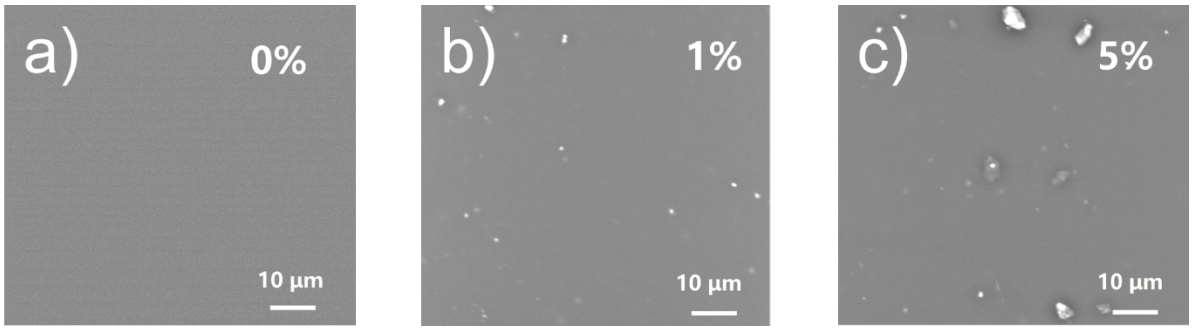

Fig. S4. SEM micrographs of the top surfaces of ZIF-72/PDMS nanocomposite films, containing a) 0 wt%, b) 2 wt%, and c) 5 wt% of ZIF-72 filler loading.

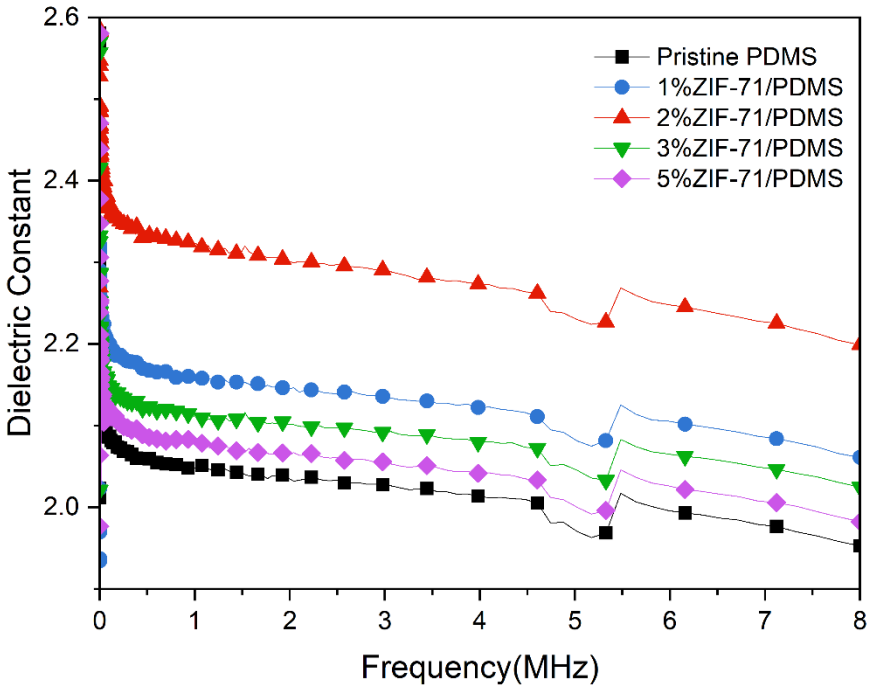

Fig. S5. Dielectric constants of ZIF-71/PDMS films at room temperature from 4 Hz to 8 MHz. The dip around 5 MHz was an artefact when the LCR meter switches its frequency range.

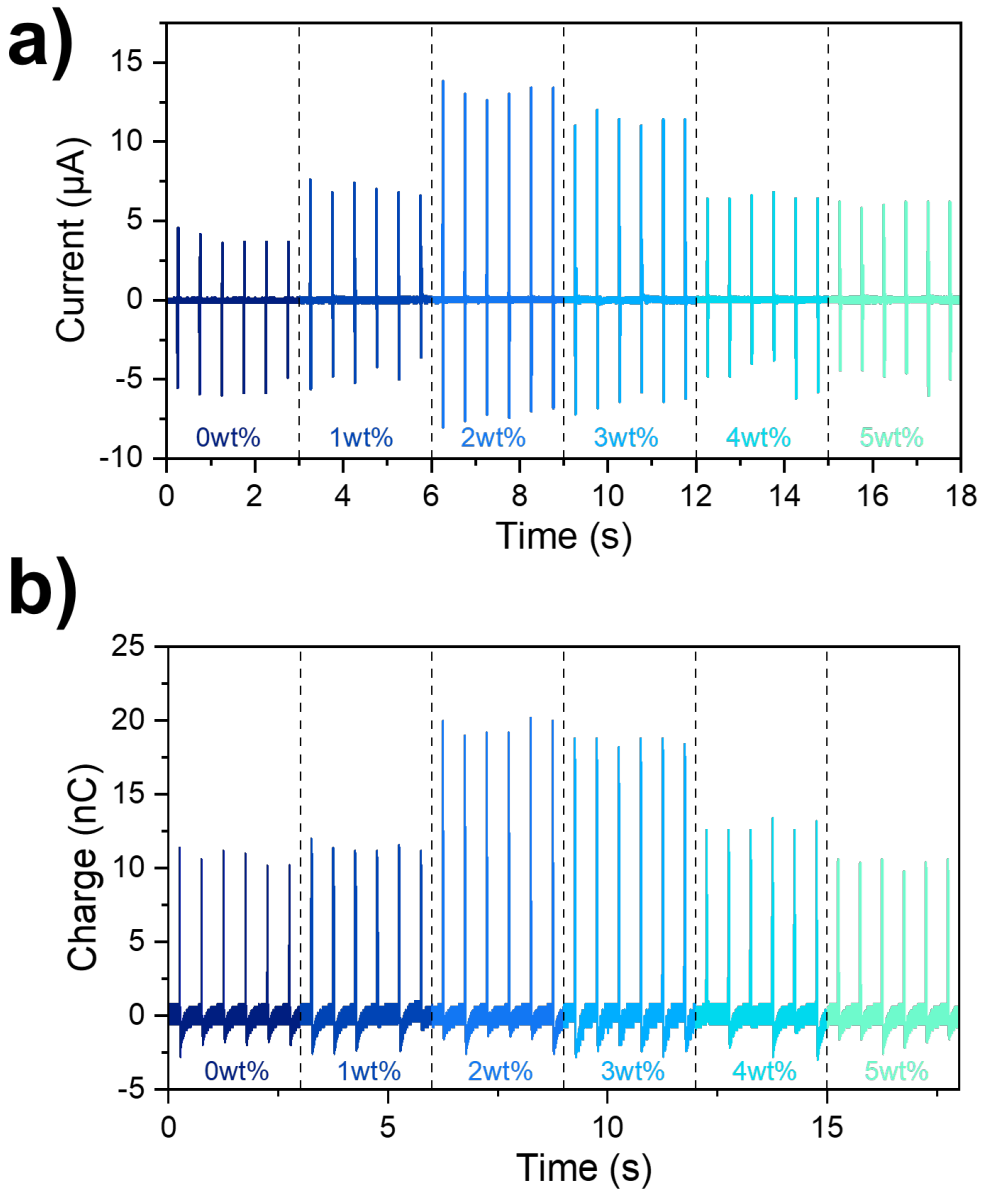

Fig. S6. a) Open-circuit current, and b) transferred charge of Z71-TENG at different mass loadings under an oscillatory motion of 2 Hz.

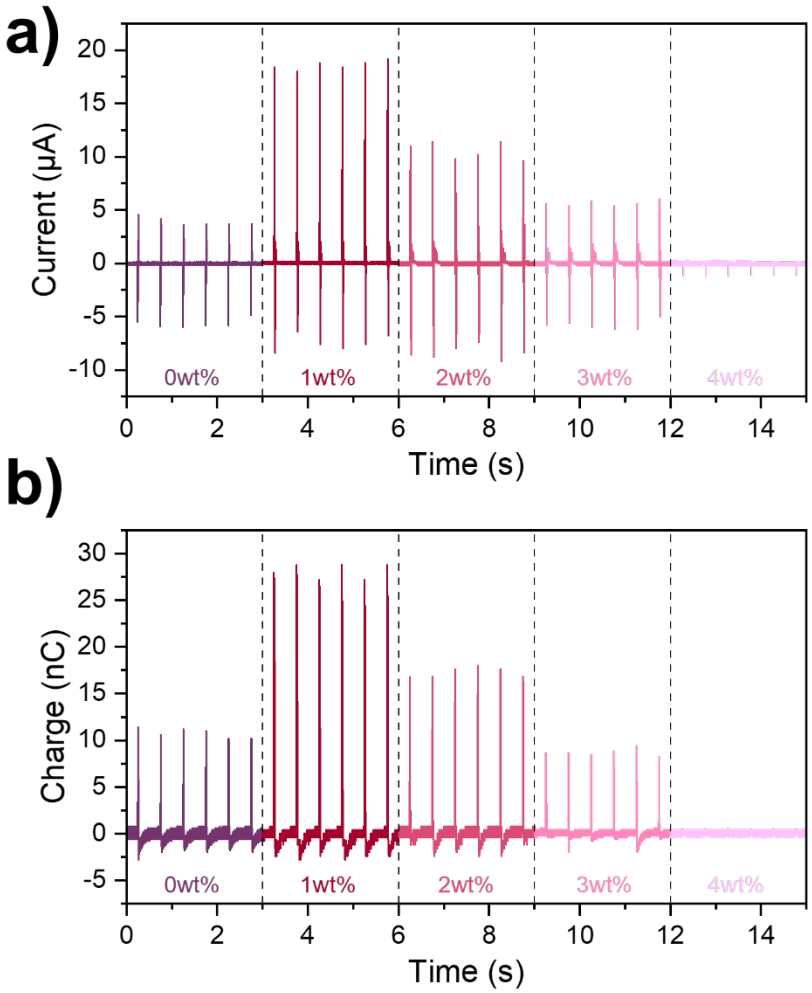

Fig. S7. a) Open-circuit current, and b) transferred charge of Z72-TENG at different mass loadings under an oscillatory motion of 2 Hz.

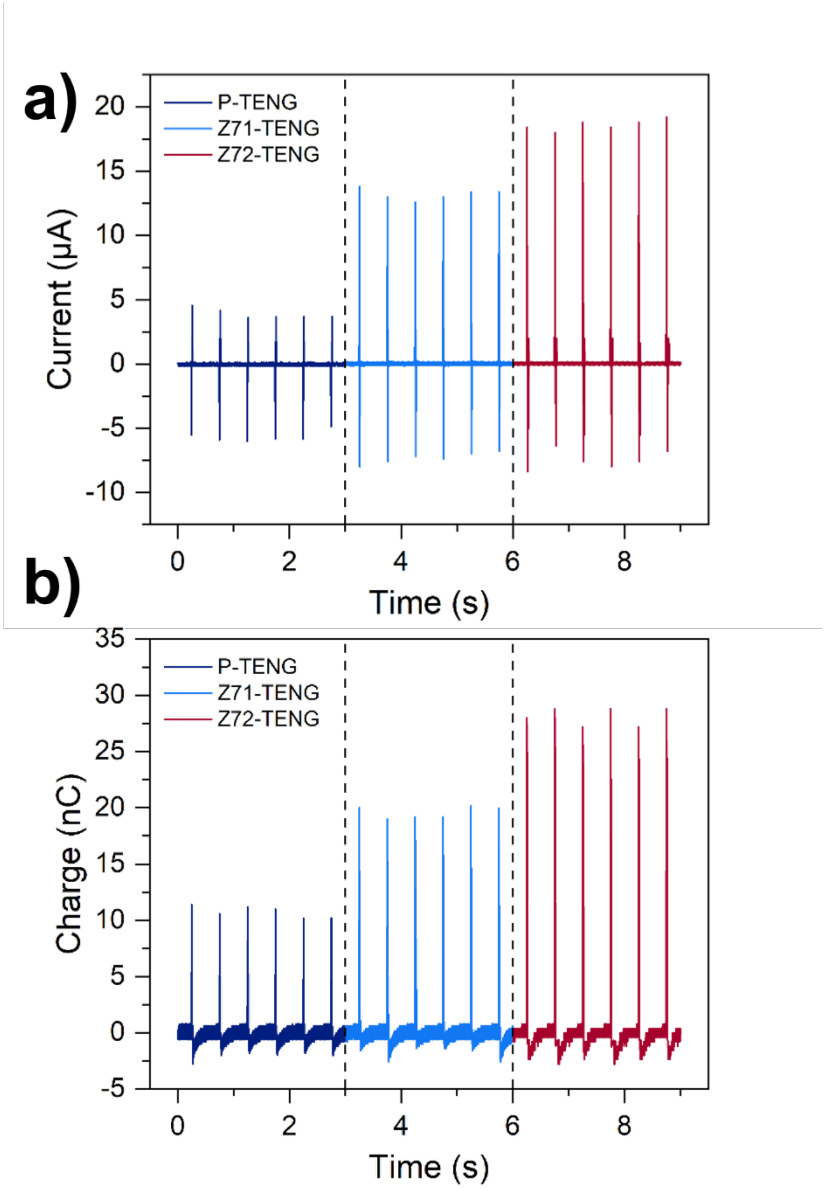

Fig. S8. Comparison of a) open-circuit current, and b) transferred charge between Z72-TENG (1 wt%), Z71-TENG (2 wt%), and P-TENG under 2 Hz oscillatory motion with 16 N impact force.

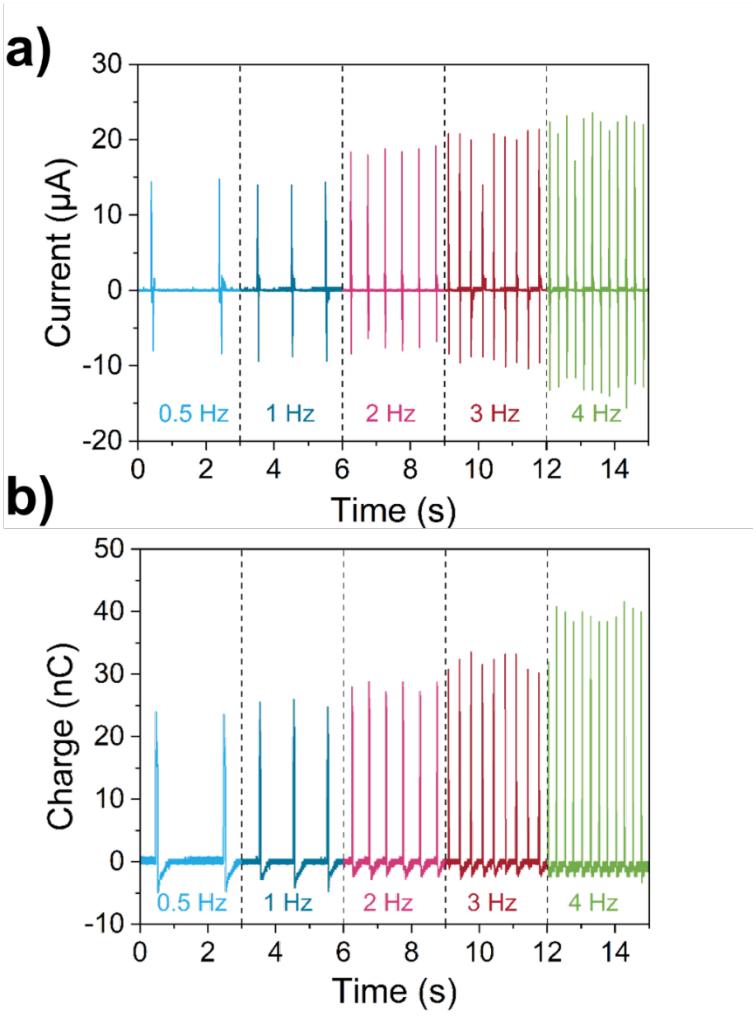

Fig. S9. a) Open-circuit current, and b) transferred charge of Z72-TENG (1 wt%) at 16 N under different frequencies.

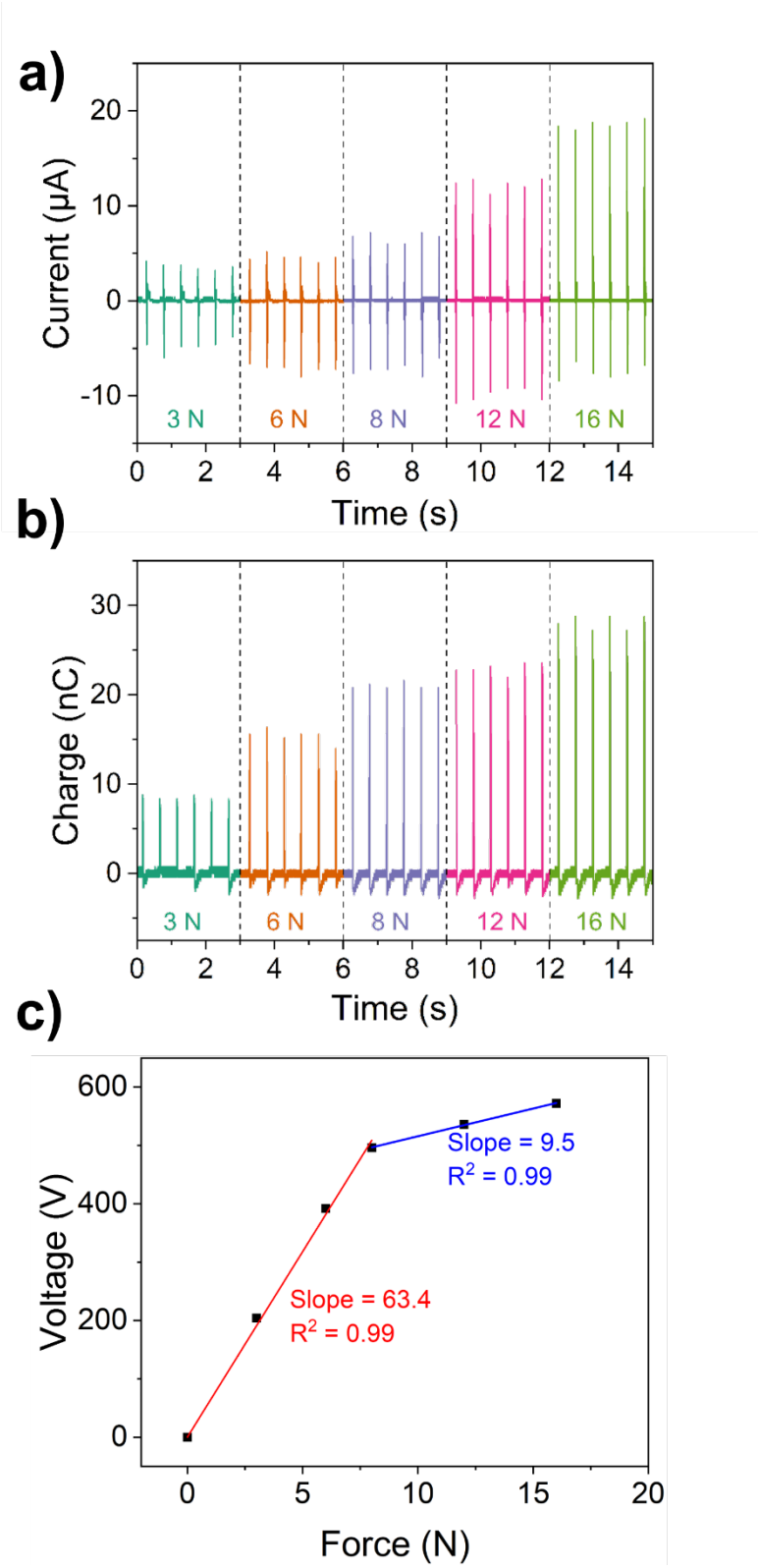

Fig. S10. a) Open-circuit current, and b) transferred charge of Z72-TENG (1 wt%) at 2 Hz subject to a varying impact force. c) Correlation between force and voltage for Z72-TENG.

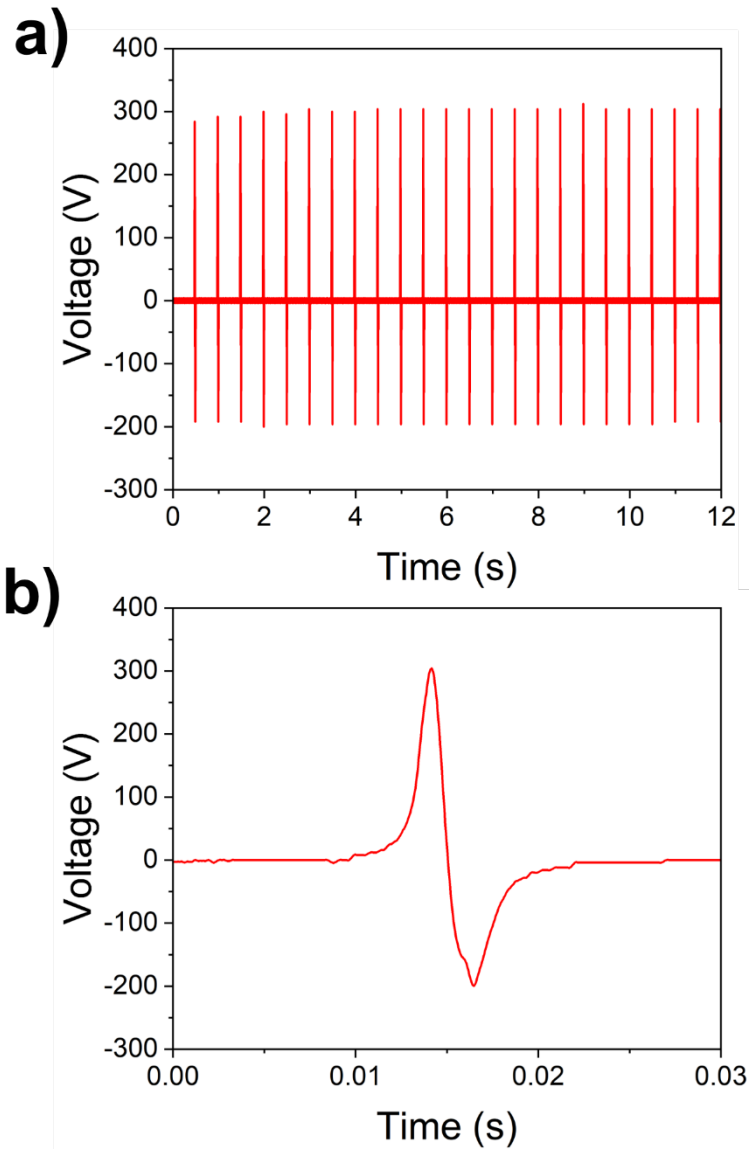

Fig. S11. a) Example of a stable open-circuit voltage output under 2 Hz. b) Magnified view of a single peak's voltage signal.

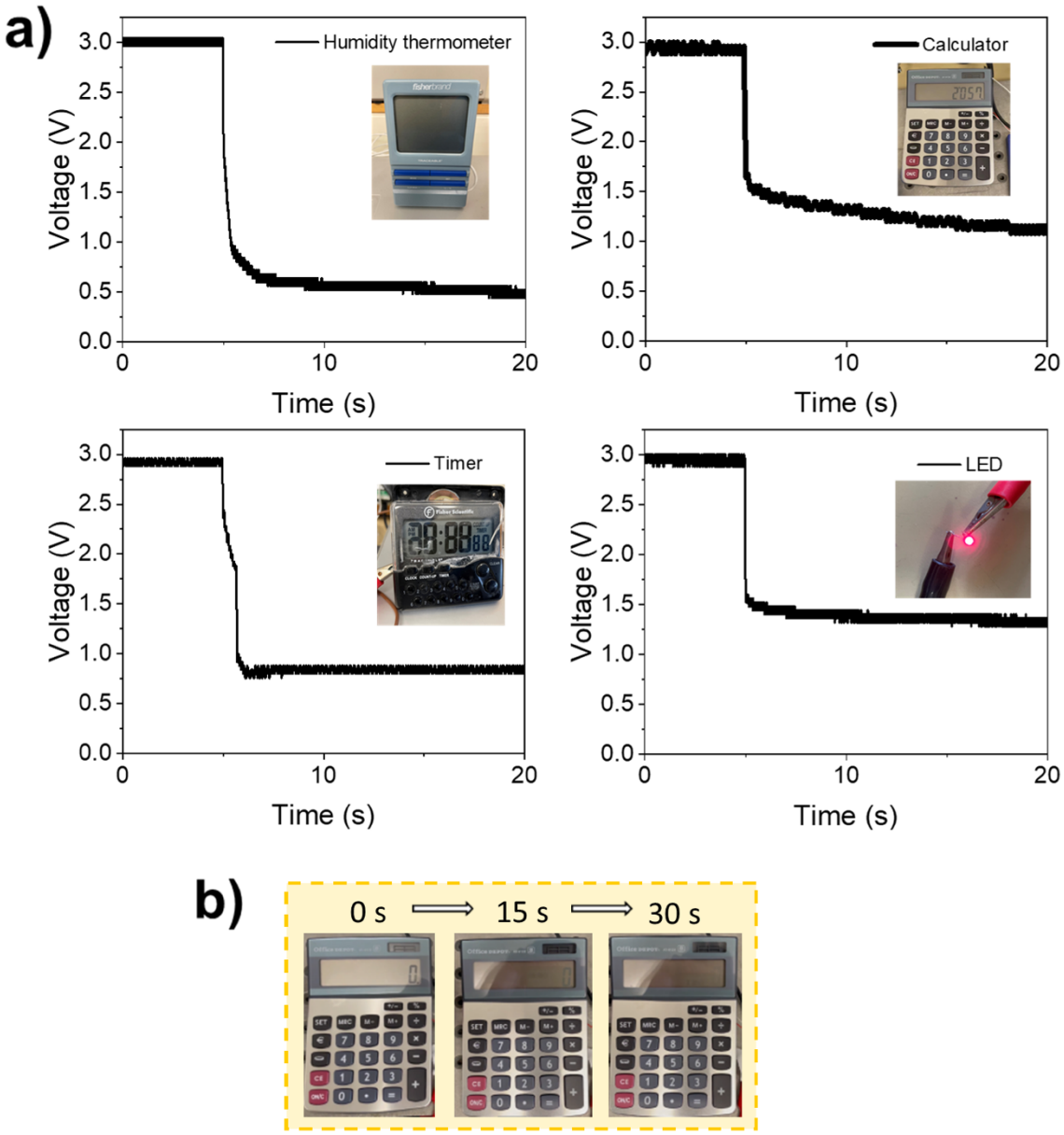

Fig. S12. a) Voltage profiles of discharging a 47 μF capacitor by four different electronic devices. b) Powering of a commercial calculator by Z72-TENG for operational times of 0, 15, and 30 s; note that the solar panel has been disconnected before testing.

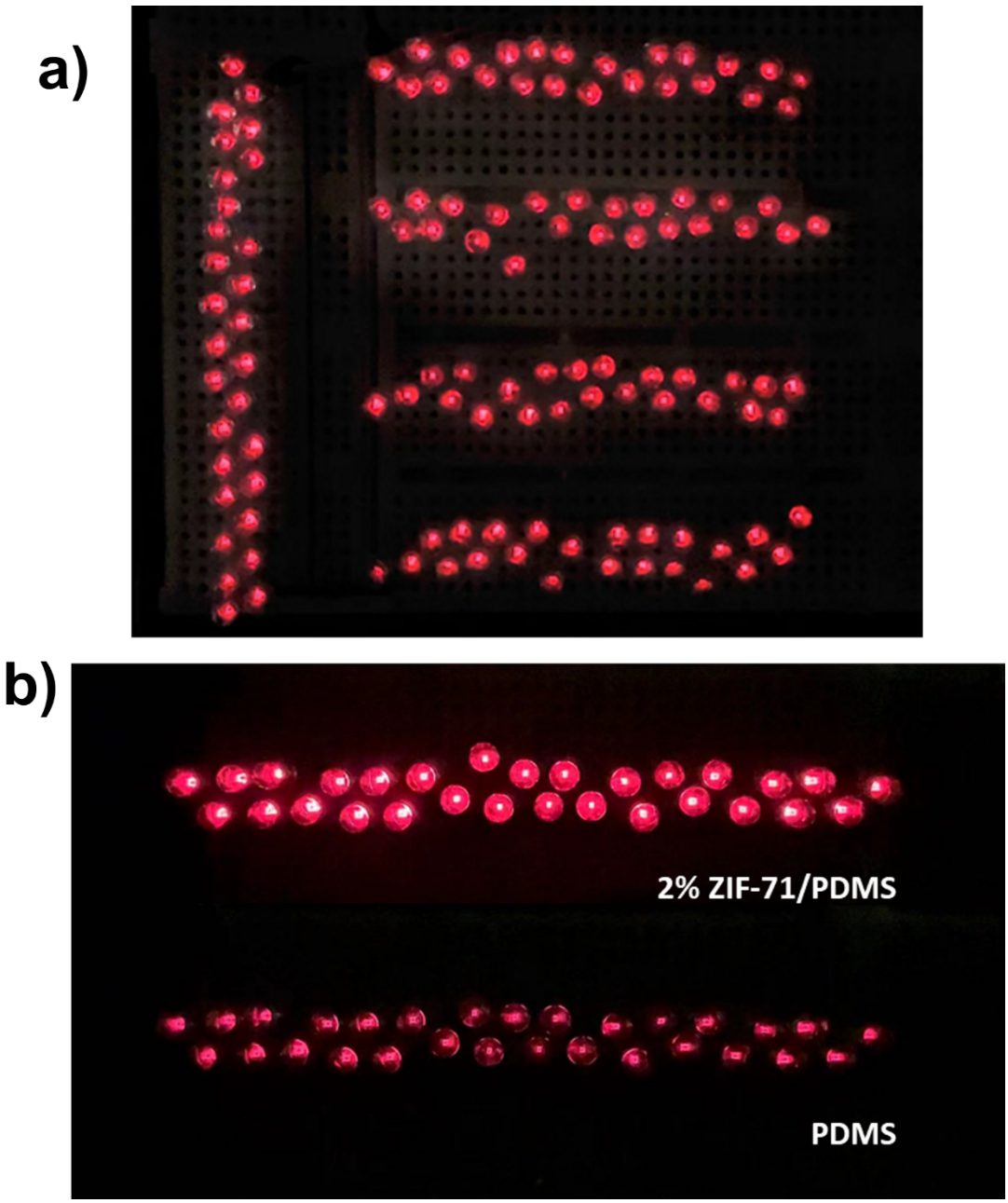

Fig. S13. a) Illumination of 120 LEDs at 2 Hz by the electricity generated from Z72-TENG. b) Difference in illumination intensities of LEDs powered by PDMS-based TENG and Z71-TENG.

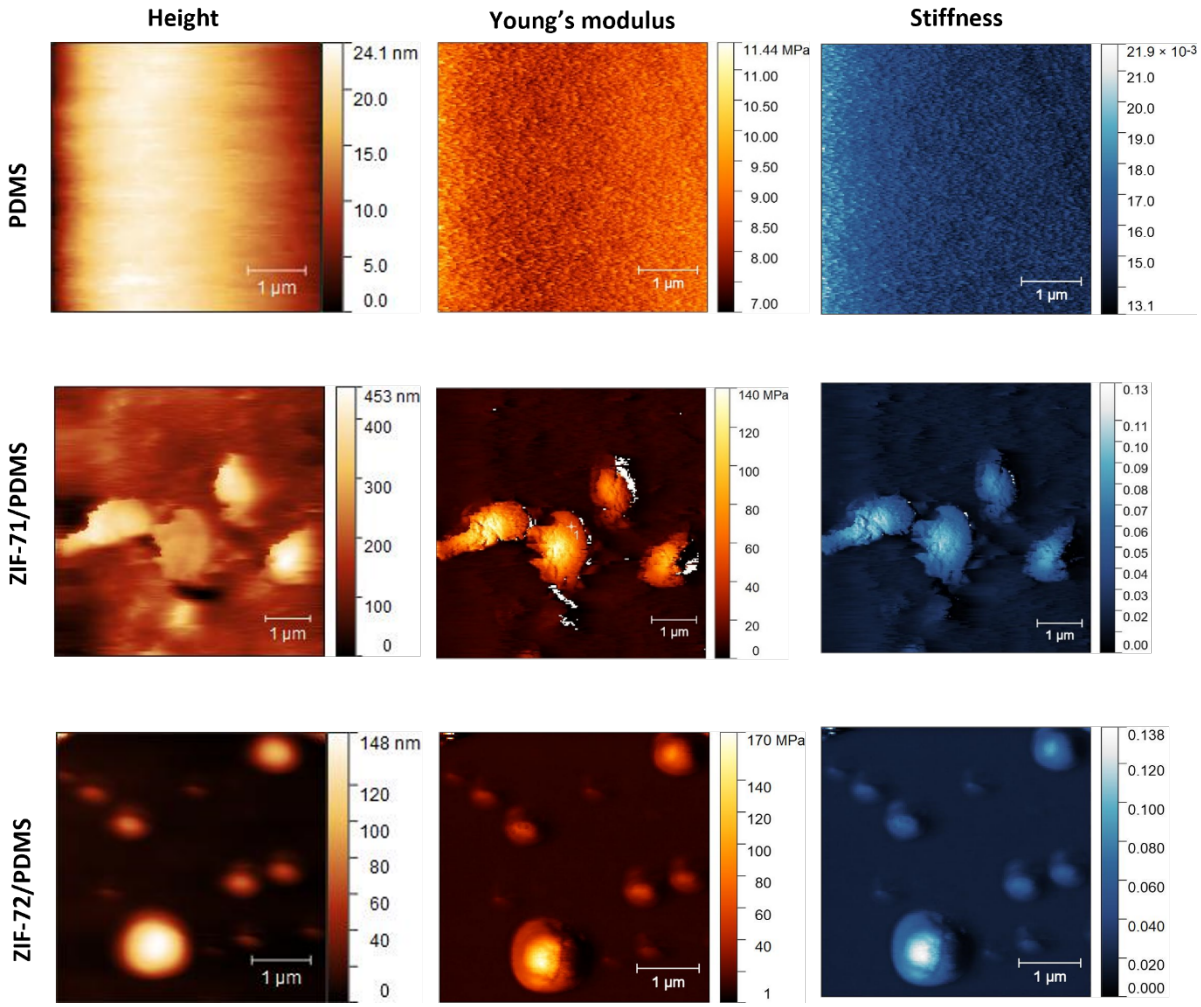

Fig. S14. Nanoscale surface characterisation of height topography, Young's modulus, and stiffness of neat PDMS, ZIF-71/PDMS, and ZIF-72/PDMS films.

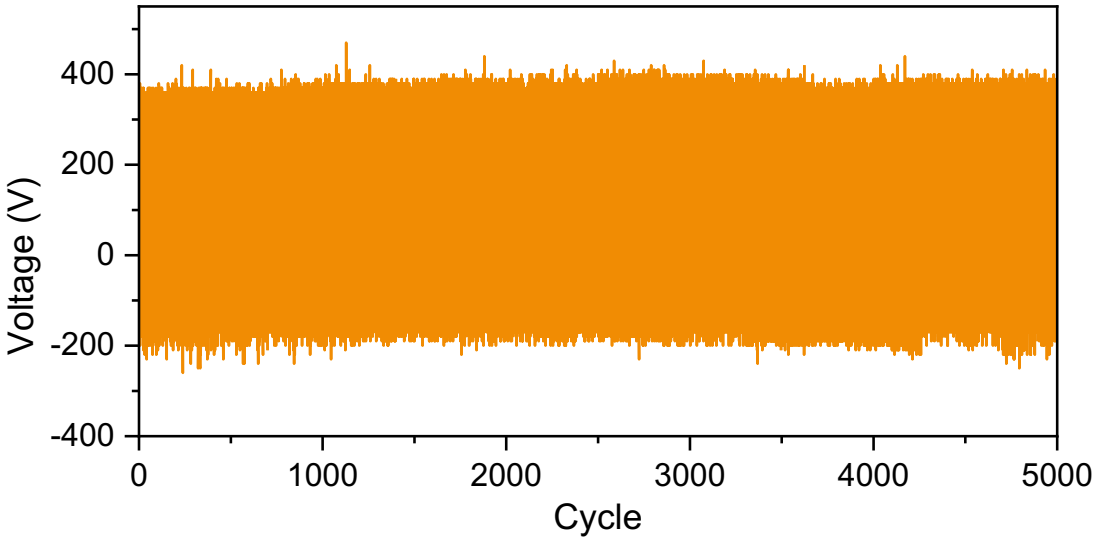

Fig. S15. Durability of Z71-TENG after a continuous run over 5,000 contact-separation oscillatory cycles.

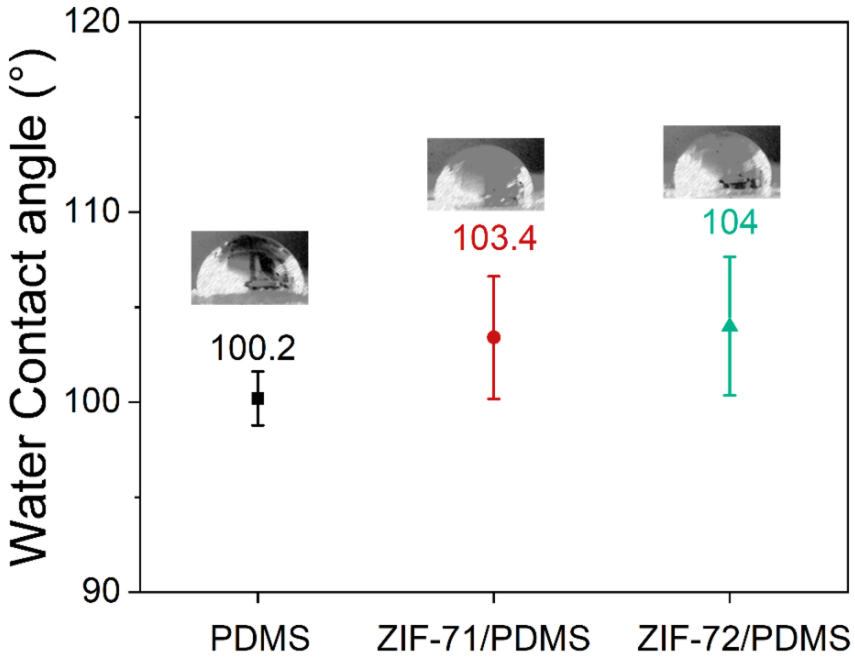

Fig. S16. Water contact angles of pristine PDMS, ZIF-71/PDMS and ZIF-72/PDMS films. Both ZIF-71/PDMS and ZIF-72/PDMS nanocomposites show improved hydrophobicity comparing with the neat PDMS film, increasing the water contact angle of PDMS film from about 100° to 104°.

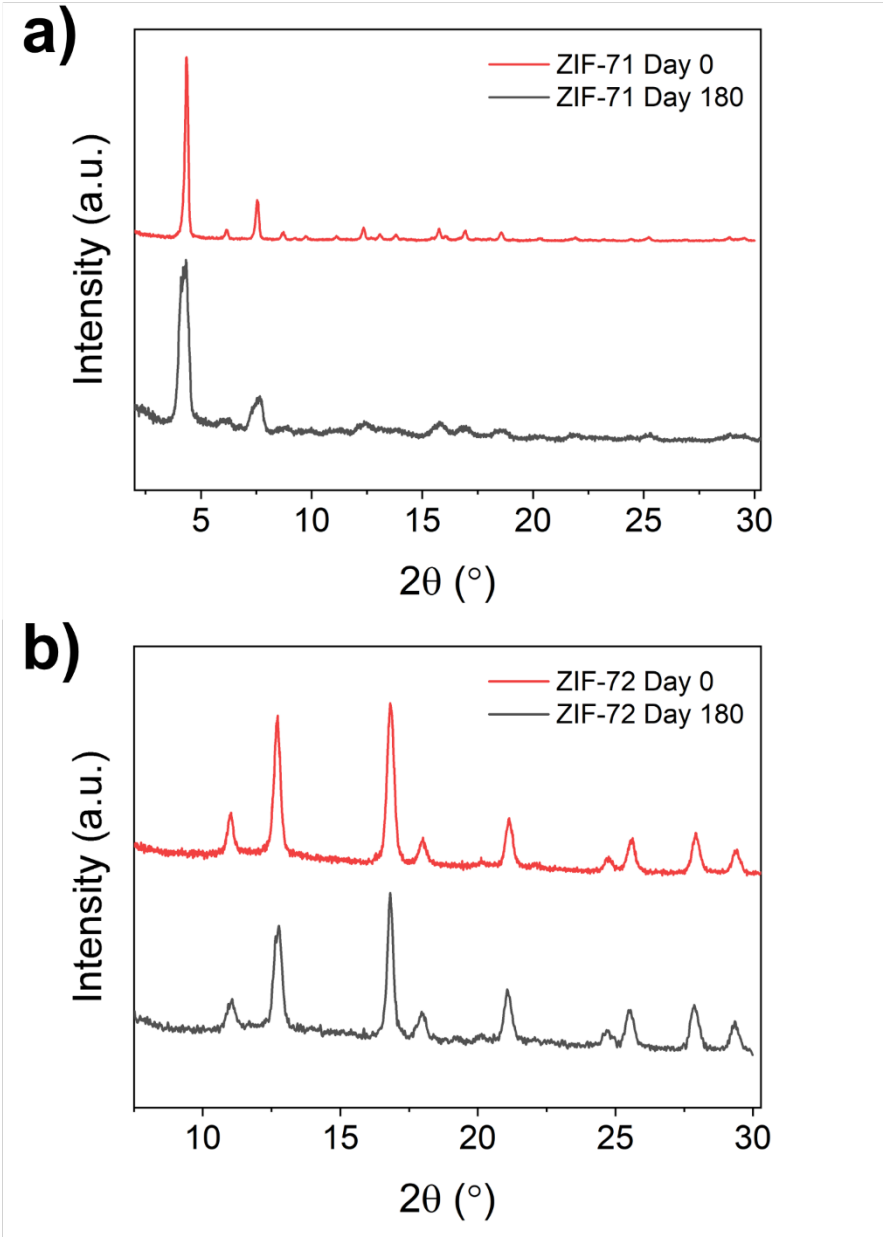

Fig. S17. Changes in XRD patterns for (a) ZIF-71 and (b) ZIF-72 nanoparticles after 180 days. Both ZIF-71 and ZIF-72 show excellent structural stability under ambient conditions (temperature and humidity), where the XRD patterns were retained despite some peak broadening observed for ZIF-71 nanoparticles.

Table S1. Comparison of current results against the electrical outputs of PDMS-based TENG devices reported in the literature. Note: P-P denotes the peak-to-peak voltage.

Name of device	**Polymer matrix**	**Filler**	**Positive layer**	**P-P Voltage, V_{oc}**	**Current, I_{sc}**	**Max Power Density**	**Reference**
Silver Nanowires TENG	PDMS	AgNW	PFA	203 V	22 μA	-	[1]
CNT–PDMS TENG	PDMS	Aligned CNT	ITO	275 V	54 μA	4700 mW m^{-2}	[2]
3D-MXene/PDMS TENG	PDMS	3D-Mxene	Nylon	65 V	0.6 μA	-	[3]
F-MOF TENG	PDMS	KAUST-8	Al	530 V	3.2 μA	520 mW m^{-2}	[4]
Perovskite-TENG	PDMS	$Sr_3CO_2WO_9$ (SCWO)	Al	300 V	2.2 μA	305 mW m^{-2}	[5]
ZIF-TENG	PDMS	ZIF-8	Cu	176 V	16.3 μA	1764 mW m^{-2}	[6]
SWCNT-IL-PDMS TENG	PDMS	SWCNT and IL	Teflon	90 V	2.5 μA	117 mW m^{-2}	[7]
Z72-TENG	**PDMS**	**ZIF-72**	**Al**	**1139 V**	**19 μA**	**5028** mW m^{-2}	**This Work**

References

1. Kang, H., et al., *Mechanically Robust Silver Nanowires Network for Triboelectric Nanogenerators.* Adv. Funct. Mater., 2016. **26**(42): p. 7717-7724.
2. Wang, H., et al., *High performance triboelectric nanogenerators with aligned carbon nanotubes.* Nanoscale, 2016. **8**(43): p. 18489-18494.
3. Wang, D., et al., *Multifunctional 3D-MXene/PDMS nanocomposites for electrical, thermal and triboelectric applications.* Compos. - A: Appl. Sci. Manuf., 2020. **130**: p. 105754.
4. Guo, Y., et al., *Fluorinated metal-organic framework as bifunctional filler toward highly improving output performance of triboelectric nanogenerators.* Nano Energy, 2020. **70**: p. 104517.
5. Sahu, M., et al., *Triple perovskite-based triboelectric nanogenerator: a facile method of energy harvesting and self-powered information generator.* Mater. Today Energy, 2021. **20**: p. 100639.
6. Wen, R., et al., *A composite triboelectric nanogenerator based on flexible and transparent film impregnated with ZIF-8 nanocrystals.* Nanotechnology, 2021. **32**(34): p. 345401.
7. Zhao, X. and Z. Ounaies, *A facile method to enhance the flexibility and triboelectric output of PDMS using ionic liquid-coated single-wall carbon nanotubes.* Nano Energy, 2022. **94**: p. 106908.